A New Class of Selective Myocardial Calcium Channel Modulators. 2. Role of the Acetal Chain in Oxadiazol-3-one Derivatives

Roberta Budriesi,*,† Emanuele Carosati,‡ Alberto Chiarini,† Barbara Cosimelli,*,§ Gabriele Cruciani,‡ Pierfranco Ioan,† Domenico Spinelli,‖ and Raffaella Spisani‖

Dipartimento di Scienze Farmaceutiche, Università degli Studi di Bologna, Via Belmeloro 6, 40126 Bologna, Italy, Dipartimento di Chimica, Università di Perugia, via Elce di Sotto 8, 06123 Perugia, Italy, Dipartimento di Chimica Farmaceutica e Tossicologica, Università degli Studi di Napoli "Federico II", Via Montesano 49, 80131 Napoli, Italy, Dipartimento di Chimica Organica "A. Mangini", Università degli Studi di Bologna, Via S. Giacomo 11, 40126 Bologna, Italy

In the framework of the continuing interest of this research group in the use of 8-aryl-8-hydroxy-8*H*-[1,4]thiazino[3,4-*c*][1,2,4]oxadiazol-3-ones (**1**) as calcium entry blockers, a number of acetals were synthesized and assayed "in vitro". All of them are structurally related to diltiazem and pyrrolobenzothiazines. The effect on the biological profile was measured by functional assays for a wide variety of acetal residues: saturated linear and branched chains, short and long unsaturated *E* and/or *Z* chains as well as benzyl and methylcyclohexyl residues. From selective assays on the most active derivative (**5b**) (EC$_{50}$ = 0.04 μM), which is 20 times more active than diltiazem (EC$_{50}$ = 0.79 μM), a muscarinic or adenosinic mechanism of action was excluded. A 3D QSAR model was obtained and validated with homologous literature data, and a virtual receptor scheme was derived for the unknown binding site. The following pharmacophoric features favorably affect the potency: one positively charged center, three lipophilic groups, and two hydrogen-bonding acceptor groups.

Introduction

We have recently described the synthesis[1,2] and the pharmacological activity[3] of a series of 8-aryl-8-hydroxy-5-methyl-8*H*-[1,4]thiazino[3,4-*c*][1,2,4]oxadiazol-3-ones that are structurally related to the well-known L-type calcium entry blocker (CEB) diltiazem (**2**) (Chart 1). Analysis of the biological data clearly reveals that all tested compounds exhibit very good negative inotropic potency and most of them show better intrinsic activity and potency than diltiazem.

Because these new compounds have a structural correlation to diltiazem, it was hypothesized that they may act as L-type calcium channel modulators on the diltiazem binding site.

L-type calcium channels exist as hetero-oligomeric complexes composed of the pore-forming α_1 subunit, the disulfide-linked α_2-δ subunit, and the intracellular β subunit. Only the skeletal muscle L-type channel has an additional transmembrane γ subunit.[4,5] The α_1 subunit is the largest one: it forms the conduction pore, the Ca^{2+} selective filter, the voltage sensor, and the known sites of channel regulation by drugs and toxins.[6] At least four distinct L-type calcium channel α_1 subunits have been cloned and characterized.[7] Some CEBs (in particular dihydropyridines) have a different affinity for various tissues (cardiac and vascular) due to their ability to discriminate between the different α_1 subunits of L-type calcium channels in various tissues.[8]

Chart 1

X = Cl, Br
a = Cl
b = Br

8-aryl-8-hydroxy-5-methyl-8*H*-[1,4]thiazino[3,4-*c*][1,2,4]oxadiazol-3-one (**1a,b**)

(+)-*cis*-Diltiazem (**2**)

On the grounds of these considerations and of the results obtained, it was hypothesized that this new series of molecules is selective for the Ca$_v$1.2a splice type of the α_1 subunit, which is expressed in the heart.[9]

Small molecules that selectively modulate the Ca^{2+} channel could have important therapeutic applications because they recognize only one target among multiple targets in different tissues. In particular, the discovery of selective molecules against cardiovascular diseases remains a formidable challenge to medicinal chemists.

The biological studies, together with previous SARs and computational data, have brought some structural features to light that improve negative inotropic activity and reduce the chronotropic and vasorelaxant effects.[3] For example, a methyl group at position 5 of the thiazino-oxadiazolone ring and an unsubstituted or *p*-Br-substituted phenyl ring at position 8 appear to be capable of increasing the pharmacological activity. Taking into account the fact that diltiazem shows significant activity (EC$_{50}$ = 0.79 μM), and with the aim of evaluating the importance of the free hemiacetalic hydroxyl at position 8, we have previously synthesized[3] **3a** and **4a** (Chart 2) from **1a**, whose activity (EC$_{50}$ = 0.80 μM) closely resembles that of **2**.

* Corresponding authors. R.B.: Tel, +39-051-2099737; fax, +39-051-2099721; e-mail, roberta.budriesi@unibo.it. B.C.: Tel, +39-081-678614; fax, +39-081-678630; e-mail, barbara.cosimelli@unina.it.
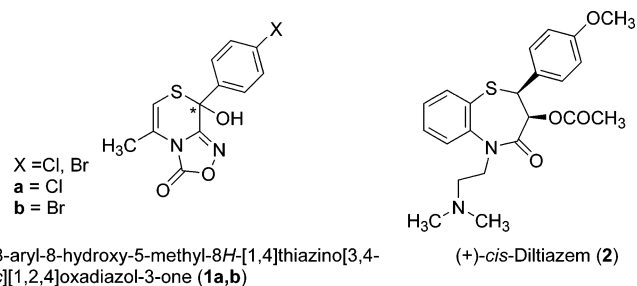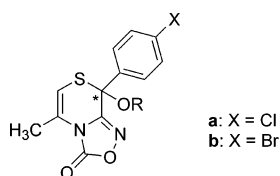† Dipartimento di Scienze Farmaceutiche, Università degli Studi di Bologna.
‡ Università di Perugia.
§ Università degli Studi di Napoli "Federico II".
‖ Dipartimento di Chimica Organica "A. Mangini", Università degli Studi di Bologna.

Chart 2

1a, b: R = H	**11a, b**: R = (CH$_2$)$_{11}$CH$_3$
3a, b: R = CH$_3$	**12a, b**: R = (CH$_2$)$_{14}$CH$_3$
4a, b: R = CH$_2$CH(CH$_3$)$_2$	**13a, b**: R = (CH$_2$)$_{17}$CH$_3$
5a, b: R = CH$_2$CH$_3$	**14a, b**: R = CH(CH$_3$)$_2$
6a, b: R = (CH$_2$)$_2$CH$_3$	**15a, b**: R = CH$_2$CH=CH$_2$
7a, b: R = (CH$_2$)$_3$CH$_3$	**16a, b**: R = CH$_2$CH=CHCH$_2$CH$_3$ (*E*-isomer)
8a, b: R = (CH$_2$)$_4$CH$_3$	**17a, b**: R = CH$_2$CH=CHCH$_2$CH$_3$ (*Z*-isomer)
9a, b: R = (CH$_2$)$_5$CH$_3$	**18a, b**: R = (CH$_2$)$_8$CH=CH(CH$_2$)$_7$CH$_3$ (*Z*-isomer)
10a, b: R = (CH$_2$)$_8$CH$_3$	**19a, b**: R = CH$_2$-Ph
	20a, b: R = CH$_2$-cyclohexyl

Interestingly, on passing from **1a** to **3a** (R = methyl, EC$_{50}$ = 1.54 μM) the potency is cut by about one-half, whereas on passing from **1a** to **4a** (R = isobutyl, EC$_{50}$ = 0.56 μM) it increases smoothly.

With the aim of obtaining an improved understanding of the SARs for compounds **1** and their derivatives and of improving negative inotropic activity, a series of acetals with different steric requirements was synthesized and evaluated (Chart 2).

It must be noted that compounds **1** contain a non-stable stereogenic center (consequently, the enantiomers cannot be separated), whereas compounds **3**–**20** contain one stable stereogenic center and in addition their enantiomers can be separated. The preliminary results concern only compound **3a** but reveal for the two enantiomers similar activity.

Several of these new compounds demonstrate negative inotropic activity and, in particular, **5b** is the most active and potent of them all. To further investigate the hypothesis that this negative inotropic effect is due to the binding of the compound at a specific site localized on L-type calcium channels, confutation was performed on some mechanisms otherwise responsible for negative inotropic activity, such as the muscarinic and the adenosine ones.

Subsequently, we applied molecular modeling techniques in order to explore the high affinity of the new structures toward the diltiazem binding site and to confirm or refine the recent hypotheses concerning its structural features. In fact, in recent years several SAR studies and quantitative models have been proposed in order to understand the binding mode of calcium antagonists and to propose receptor site schemes for all the three major antagonist classes, that is, BTZs,[10–15] DHPs,[16,17] and PAAs.[18] Despite the abundance of models regarding DHP-type, little information is available concerning the binding mode of BTZ diltiazem analogues.

In the early 1990s, Floyd et al.[10] demonstrated that the calcium channel blocking activity of benzazepinones, which are molecules isosterically related to benzothiazepines (diltiazem), is dependent upon two pharmacophores: a hydrogen-bond acceptor and a basic residue. In the late 1990s Campiani et al.[11–13] presented a 3D QSAR study on pyrrolobenzothiazines using the CoMFA methodology. They found two hydrogen-bonding sites, two lipophilic regions, and one basic center. Similarly, Kettman and Höltje[14] proposed a five-point pharma-

cophore hypothesis, while Schleifer and Tot[15] characterized a pharmacophore model composed of two aromatic ring systems, a basic center, and a methoxy group.

This paper reports a quantitative structure–activity relationship study of the set of acetals described in Table 1, integrated by addition of some of the molecules described in refs 3 and 11. To extract structural features related to the negative inotropic potency, molecular descriptors based on the GRID force field[19,20] were used, namely, *g*rid-*in*dependent *d*escriptors (GRIND).[21] These have been introduced in the field of 3D QSAR to overcome the main drawback of any CoMFA-like approach, i.e., the alignment of compounds, which causes major disadvantages as to the treatment of stereogenic centers.

The 3D QSAR model derived was successfully validated by using an external set of 15 homologous and structurally similar compounds, with comparable inotropic potency. Hence, the model would be used to forecast the potency of further BTZs analogues. Furthermore, a 3D pharmacophoric scheme was hypothesized, resembling the generic diltiazem binding site: the most relevant features, in agreement with the known receptor site schemes, would be used for database mining to identify novel classes of selective calcium channel blockers. However, this is beyond the scope of the present paper.

Chemistry

The synthesis of compounds **1a**,[1] **1b**,[1] **3a**,[3] and **4a**[3] has been previously reported.

Compounds **5a**–**20a** and **3b**–**20b** were usually prepared[3] from **1a** or **1b** and the proper alcohol in the presence of catalytic amounts of *p*-toluenesulfonic acid in refluxing toluene (Scheme 1).

Scheme 1
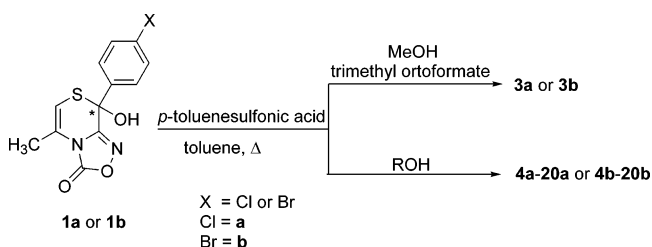
Pharmacology

Functional Studies. The pharmacological profile of all compounds was tested on guinea pig isolated left and right atria to evaluate their inotropic and chronotropic effects, respectively, and on K$^+$-depolarized guinea pig aortic strips to assess calcium antagonist activity. Guinea pig isolated left papillary muscle was employed to assess the ventricular inotropic effect of **5b** and of the reference compound diltiazem. Compounds were checked at increasing doses in order to evaluate the percentage decrease of developed tension on isolated left atrium and papillary muscle driven at 1 Hz (negative inotropic activity), the percentage decrease in atrial rate on spontaneously beating right atrium (negative chronotropic activity), and the percentage inhibition of calcium-induced contraction on K$^+$-depolarized aortic strips (vasorelaxant activity).

Table 1. Cardiovascular Activity (mean ± SEM) of Tested Compounds

compd[d]	negative inotropic activity,[a] % decrease	negative chronotropic activity,[b] % decrease	negative inotropic potency EC$_{50}$[e] (μM)	(95% cl)[f]	vasorelaxant activity,[c] % decrease
1a[g]	80 ± 4.1[h]	18 ± 1.8	0.80	(0.65−1.05)	26 ± 1.4
1b[g]	97 ± 3.7	18 ± 1.0	0.32	(0.23−0.43)	12 ± 0.6
2[i]	78 ± 3.5[h]	94 ± 5.6[j]	0.79	(0.70−0.85)	88 ± 2.3[h]
3a[g]	62 ± 2.5	22 ± 1.1	1.54	(1.21−1.88)	14 ± 0.9
3b	38 ± 2.6[j]	9 ± 0.1[h]			13 ± 0.7
4a[g]	83 ± 1.2	15 ± 0.5	0.56	(0.39−0.79)	37 ± 1.5
4b	79 ± 1.5[h]	11 ± 0.9	0.31	(0.24−0.39)	6 ± 0.3
5a	53 ± 0.6[l]	16 ± 0.2	0.27	(0.14−0.45)	28 ± 1.4
5b	77 ± 1.7[j]	5 ± 0.2[h]	0.04	(0.03−0.05)	19 ± 0.9
6a	73 ± 2.1	7 ± 0.2	0.89	(0.69−1.10)	20 ± 1.9
6b	69 ± 2.7	12 ± 0.5	0.41	(0.34−0.49)	14 ± 0.5
7a	62 ± 5.2	9 ± 0.3	1.85	(1.55−2.20)	9 ± 0.5
7b	82 ± 5.3	18 ± 1.4	1.02	(0.88−1.35)	2 ± 0.1
8a	45 ± 1.5	14 ± 1.1			15 ± 0.7
8b	34 ± 3.1	2 ± 0.1			3 ± 0.2
9a	68 ± 3.1	10 ± 0.9	0.64	(0.53−0.81)	3 ± 0.2
9b	81 ± 2.5	9 ± 0.5	0.83	(0.79−0.84)	2 ± 0.1
10a	73 ± 3.5	11 ± 0.7	0.79	(0.54−1.15)	4 ± 0.2
10b	71 ± 3.6[l]	7 ± 0.1	0.35	(0.27−0.44)	3 ± 0.1
11a	56 ± 3.4	5 ± 0.3	0.87	(0.59−1.26)	5 ± 0.2
11b	59 ± 1.2[h]	16 ± 0.9	0.13	(0.09−0.15)	3 ± 0.2
12a	69 ± 3.2	9 ± 0.8	1.13	(0.91−1.27)	3 ± 0.2
12b	75 ± 2.4	12 ± 0.9	0.42	(0.28−0.64)	4 ± 0.2
13a	39 ± 2.6	15 ± 0.7[h]			2 ± 0.1
13b	66 ± 3.4	5 ± 0.3	0.97	(0.68−1.21)	6 ± 0.3
14a	64 ± 1.9[l]	10 ± 0.9	0.22	(0.16−0.28)	10 ± 0.4
14b	58 ± 2.7[h]	4 ± 0.3	0.27	(0.21−0.33)	18 ± 0.9
15a	84 ± 3.1	13 ± 0.9	0.37	(0.20−0.69)	21 ± 1.5
15b	91 ± 1.3	13 ± 0.8	0.55	(0.46−0.68)	13 ± 0.7
16a	46 ± 2.1	8 ± 0.5			10 ± 0.9
16b	43 ± 1.3	10 ± 0.3			11 ± 0.9
17a	67 ± 2.4	5 ± 0.2	1.31	(0.97−1.43)	10 ± 0.8
17b	81 ± 2.9	20 ± 1.1	0.63	(0.45−0.80)	11 ± 0.8
18a	70 ± 2.5	14 ± 0.9	0.87	(0.58−1.35)	7 ± 0.3
18b	84 ± 1.4	9 ± 0.7	1.26	(0.89−1.53)	2 ± 0.1
19a	63 ± 0.2	5 ± 0.3	0.74	(0.69−0.96)	4 ± 0.1
19b	63 ± 1.5	4 ± 0.1	0.59	(0.48−0.67)	2 ± 0.1
20a	55 ± 2.3	5 ± 0.2	0.24	(0.19−0.31)	5 ± 0.4
20b	78 ± 1.3	8 ± 0.4	0.19	(0.15−0.25)	3 ± 0.2

[a] Activity means the decrease in developed tension in isolated guinea pig left atrium at 5×10^{-5} M, expressed as percentage changes from the control ($n = 4-6$). The left atria were driven at 1 Hz. The 5×10^{-5} M concentration gave the maximum effect for most compounds. [b] Activity means decrease in atrial rate in guinea pig spontaneously beating isolated right atria at 5×10^{-5} M, expressed as percentage changes from the control ($n = 6-8$). Pretreatment heart rate ranged from 170 to 195 beats/min. The 5×10^{-5} M concentration gave the maximum effect for most compounds. [c] Activity means the percentage inhibition of calcium−induced contraction on K$^+$-depolarized guinea pig aortic strip at 5×10^{-5} M. The 5×10^{-5} M concentration gave the maximum effect for most compounds. [d] Dataset molecules with the exception of diltiazem (**2**) were synthesized and pharmacologically evaluated in their racemic form. [e] Calculated from log concentration− response curves (Probit analysis according to Litchfield and Wilcoxon[22] with $n = 6-8$). When the maximum effect was <50%, the EC$_{50}$ inotropic, EC$_{30}$ chronotropic, and IC$_{50}$ values were not calculated. [f] Confidential limits. [g] Reference 3. [h] At 10^{-5} M. [i] EC$_{30}$ = 0.07 (cl: 0.064− 0.075), IC$_{50}$ = 2.6 (cl: 2.2−3.1). [j] At 10^{-6} M. [k] At 10^{-4} M. [l] At 5×10^{-6} M.

The functional activity at muscarinic M$_2$ and adenosine A$_1$ receptor subtypes was evaluated on driven guinea pig left atria by constructing cumulative concentration− response curves for **5b** after incubation for 60 min with 1 μM atropine (M$_2$-muscarinic receptor antagonist) or 1 μM 8-cyclopentyl-1,3-dipropylxanthine (DPCPX) (A$_1$-adenosine receptor antagonist), which were compared with those obtained in the absence of antagonist.

According to Langendorff, the guinea pig isolated perfused heart was used to assay the whole cardiac activity of compound **5b** and of the reference diltiazem. Compounds were checked at increasing doses to evaluate changes in left ventricular pressure (inotropic activity), heart rate (chronotropic activity), coronary perfusion pressure (coronary activity), and electrocardiogram (ECG) signal.

Data were analyzed using Student's *t*-test. The potency of drugs, defined as EC$_{50}$, EC$_{30}$, and IC$_{50}$, was evaluated from log concentration−response curves (Pro-bit analysis using Litchfield and Wilcoxon[22] or Graph-Pad Prism software[23,24]) in the appropriate pharmacological preparations. All data are presented as mean ± SEM.[24]

Results and Discussion

Pharmacological Characterization and Qualitative SAR Analysis. For compounds listed in Chart 2, their efficacy and potency on driven left atria, on spontaneously beating right atria, and on smooth muscle aortic vessels are reported in Table 1. The relevant activities will be discussed in comparison with those of diltiazem.

As negative inotropic agents, several of the compounds examined exhibit higher negative inotropic potencies compared to diltiazem, whereas the negative chronotropic and vasorelaxant activities were always lower than those of diltiazem. In particular, at the maximum concentration used (50 μM) none of the tested
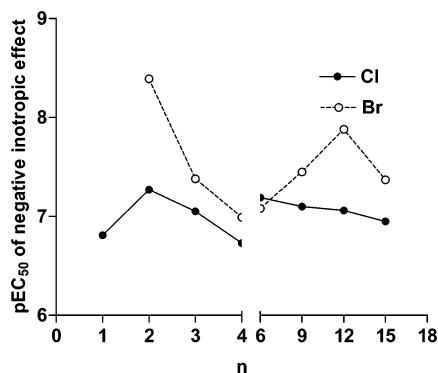
Figure 1. Effect of the carbon chain length on negative inotropic potency. EC_{50} from Table 1 were converted into pEC_{50}. $pEC_{50} = -\log EC_{50}$.

compounds showed either negative chronotropic or vasorelaxant activities higher than 30%.

The preliminary results of **3a**[3] and **4a**[3] were intriguing for their absence of the hydroxyl group which occurred in most of the compounds structurally related to diltiazem or to benzothiazine derivatives.[11–13,25–27] These results prompted the authors to explore the effect on the negative inotropic activity of an acetal moiety at 8-position. Thus, this paper reports the cardiovascular characterization of two novel series of [1,4]thiazino[3,4-*c*][1,2,4]oxadiazol-3-ones (**a** and **b** series, see Chart 2), and the 3D QSAR model derived on the cardiovascular data.

First, we synthesized and tested new acetals (**5a**–**13a**) with linear aliphatic saturated chains of increasing length bound to the oxygen at C-8. Modifying **3a** to **5a**, i.e., replacing methyl by ethyl, increases the potency about 6-fold (R = ethyl, $EC_{50} = 0.27$ μM), whereas further lengthening the chain as in **6a** (R = *n*-propyl, $EC_{50} = 0.89$ μM) and in **7a** (R = *n*-butyl, $EC_{50} = 1.85$ μM) causes a decrease in potency up to lacking potency for **8a** (R = *n*-pentyl). Interestingly, however, further lengthening as in **9a** (R = *n*-hexyl, $EC_{50} = 0.64$ μM) resulted in a slight recovery of potency.

To deeply evaluate the influence of long linear saturated chains we also tested the compounds **10a**–**13a**; passing from **10a** to **13a**, the potency smoothly falls to zero (**10a**, R = *n*-nonyl, $EC_{50} = 0.79$ μM; **11a**, R = *n*-dodecyl, $EC_{50} = 0.87$ μM; **12a**, R = *n*-pentadecyl, $EC_{50} = 1.13$ μM; **13a**, R = *n*-octadodecyl, EC_{50} = not calculated according to Table 1), suggesting an increasing filling up of the binding site. Screening these first results, the highest potency is observed with a two-carbon chain (**5a**) (Figure 1): the chain length seems to affect the potency more than the steric hindrance does.

To confirm this hypothesis, we synthesized and tested new acetals containing (a) a branched chain, namely an isopropyl residue (**14a**); (b) short or long unsaturated linear chains, either in the *E*- and/or *Z*-configuration (**15a**-**18a**); (c) a benzylic group (**19a**); and (d) a methylcyclohexyl group (**20a**).

We observed a strictly similar potency and intrinsic activity between **14a** (R = isopropyl, $EC_{50} = 0.22$ μM) and **5a**. This result underlines that the presence of a C-2 chain in the acetal system represents a useful structural manipulation to obtain high potency derivatives.

Afterward, some interesting results were collected on unsaturated acetals. For example, the potency of **15a** (R = allyl, $EC_{50} = 0.37$ μM), containing a three-atom carbon chain "frozen" around a double bond, closely resembles those of **6a** (R = *n*-propyl) and **5a** (R = ethyl). On the other hand, special interest concerned the biological data of **16a** (R = 2-pentenyl, *E*-isomer) and **17a** (R = 2-pentenyl, *Z*-isomer): a different behavior was expected due to the different arrangements that the *E*- and *Z*-chains are likely to adopt in the specific site. The chain of the *E*-isomer (**16a**) should take up about the same space as the saturated chain of **8a** (an inactive compound): accordingly, **16a** was found to be inactive. In contrast, the folded chain of the *Z*-isomer (**17a**) should allow a better accommodation in the receptor site, since it is well-known (see also the discussion on **18a**) that a folded chain (*Z*-isomer) is less space-demanding than a constrained chain with an *E*-configuration. Accordingly, an appreciable potency ($EC_{50} = 1.31$ μM) was observed between those of **6a** (C-3 chain) and **7a** (C-4 chain).

The interpretation of the above-discussed data concerning **8a**, **16a**, and **17a** is strongly supported by comparing the potency of **18a** with the inactive compound **13a**; both **13a** and **18a** contain a C-18 chain. The potency of **18a** ($EC_{50} = 0.87$ μM) is similar to those of **10a** and **11a**, which contain saturated C-9 and C-12 chains, respectively. This behavior was expected due to a precedent coordinate study of the interactions between several phosphate esters or their sodium salts with β-cyclodextrin by means of different techniques. In fact, some of us have observed[28] that oleyl phosphates (containing a C-18 linear unsaturated chain, *Z*-isomer) resemble phosphates with a C-8–C-9 chain rather than octadecyl phosphates (containing a C-18 linear saturated chain).

Last, compounds **19a** and **20a**, containing a benzyl or a methylcyclohexyl group, showed acceptable potencies ($EC_{50} = 0.74$ and 0.24 μM, respectively), despite the steric constraints due to the rigid aromatic ring and the flexible saturated six-membered ring. The occurrence of a high potency, notwithstanding the significant hindrance caused by the rings, appears very interesting: we hypothesized the higher flexibility of the cyclohexyl ring to favor a better accommodation into the active site and consequently to explain the higher potency of **20a** with respect to **19a**.

The higher activity and potency of compound **1b** versus **1a** prompted us to synthesize analogues **3b**–**20b** starting from **1b**. Their pharmacological pattern resembled that of the **a** series, with an average added value of 35%. Expectedly, compound **5b** (R = ethyl, EC_{50} = 0.04 μM), containing a C-2 chain, was the most potent within the series, being 7 and 20 times more potent than **5a** and diltiazem.

As mentioned before, this new class of compounds exhibits selective negative inotropic activity with respect to negative chronotropic and vasorelaxant ones. This peculiar cardiovascular profile was more deeply investigated by comparing the effect of diltiazem and compound **5b** on both the left papillary muscle and the isolated perfused heart according to the method of Langendorff. Diltiazem decreased the developed tension on the left papillary muscle ($EC_{50} = 1.61$ μM) as was

Table 2. Negative Inotropic Potencies of Diltiazem and **5b** on Guinea Pig Left Atria and on Guinea Pig Left Ventricular Papillary Muscle Preparations

compd	negative inotropic potency on left atria[a]		negative inotropic potency on left ventricular papillary muscle[b]		selectivity ratio[c]
	EC_{50}^d (μM)	(95% cl)[e]	EC_{50}^d (μM)	(95% cl)[e]	
2	0.79	(0.70−0.85)	1.61	(1.18−2.19)	2.04
5b	0.04	(0.03−0.05)	na[f]		

[a] Taken from Table 1. [b] Decrease in developed tension in isolated guinea pig left ventricular papillary muscle driven at 1 Hz. [c] The negative inotropic selectivity ratio was calculated as [EC_{50} for negative inotropic potency on left atrium]/[EC_{50} for negative inotropic potency on left ventricular papillary muscle]. [d] Calculated from log concentration−response curves (Probit analysis according to Litchfield and Wilcoxon[22] with $n = 5–7$). [e] Confidential limits. [f] Not active.
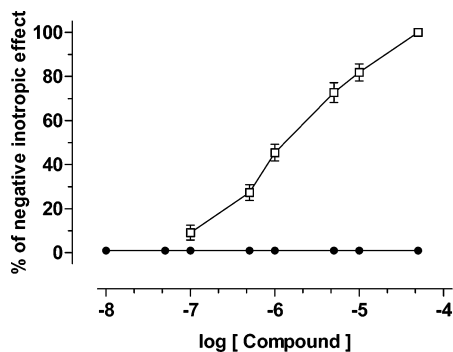
Figure 2. Concentration−response curves for the negative inotropic response of guinea pig left ventricular papillary muscles to diltiazem (□) and **5b** (●). The preparation was constantly stimulated at 1 Hz. Contractile force in the presence of different concentrations of drugs was expressed as a percentage of negative inotropic effect. The data are shown as mean ± SE from four experiments.

Table 3. Cardiac Parameters Evaluated in the Isolated Perfused Guinea Pig Spontaneously Beating Heart

compd	cardiac parameters	% change[a]	pEC$_{50}$ (95% cl)[b]
2	+(dP/dt)$_{max}^c$	−59 ± 4.2	8.03 (8.21−7.90)
	HR[d]	−25 ± 1.9	
	CPP[e]	−51 ± 3.1	7.66 (7.80−7.03)
	PQ[f]	+34 ± 2	
5b	+(dP/dt)$_{max}^c$	−3 ± 0.2	
	HR[d]	−14 ± 0.8	
	CPP[e]	−9 ± 0.5	
	PQ[f]	+32 ± 1.6	

[a] Percentage change of the basal value at the highest concentration tested (1 μM). Each value corresponded to the mean ± SEM. [b] pEC$_{50}$ = −log EC$_{50}$ calculated from log concentration−response curves (GraphPad Prism Software,[23,24] $n = 4–6$); cl, confidential limits. [c] +(dP/dt)$_{max}$: maximal rate of the rise in left ventricular pressure. [d] HR: heart rate calculated from ECG signal. [e] CPP: coronary perfusion pressure. [f] PQ: atrioventricular conduction time.

expected, whereas compound **5b** was revealed to be inactive (Table 2, Figure 2).
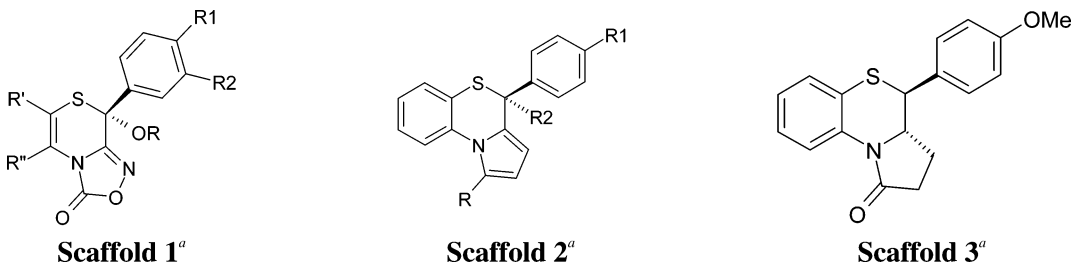
In addition to negative inotropic and chronotropic activities and coronary relaxation on the isolated perfused heart according to Langendorff, CEBs produce ECG alterations such as prolongation of atrioventricular conduction time (PQ interval) and ventricular repolarization time (QT interval). On the contrary, **5b** did not significantly influence heart rate, left ventricular contractile force, and coronary perfusion pressure in the Langendorff model. Concerning the ECG parameters, **5b** prolonged the PQ interval, as CEBs and most antiarrhythmic drugs do (Table 3).

To attribute the negative inotropic potency to the block of L-type calcium channels, other possible mech-
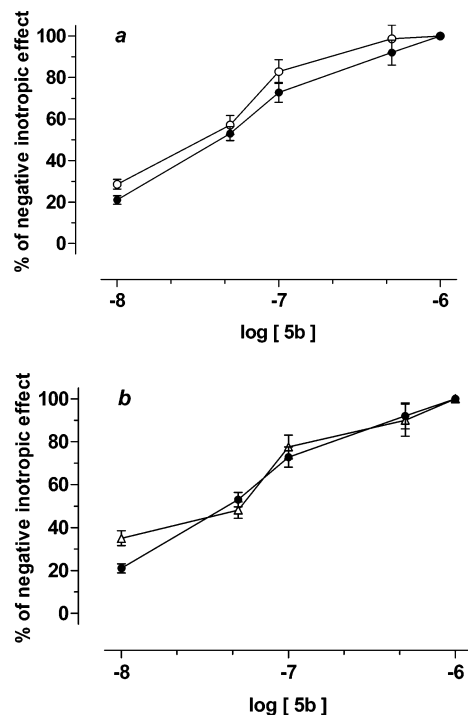
Figure 3. Cumulative concentration−response curves for **5b** (●) in absence and in the presence of atropine (1 μM) (○) (a) and DPCPX (1 μM) (△) (b) in electrically paced (1 Hz) guinea pig left atria. Each point is the mean ± SEM of four to six experiments.

anisms of negative inotropy, such as muscarinic and adenosinic, were excluded. Hence, compound **5b** was separately tested in the presence of the muscarinic antagonist atropine (1 μM) or the A$_1$ antagonist DPCPX (1 μM) (Figure 3). In both cases the EC$_{50}$ values of **5b** were not significantly different from the control, and neither atropine (EC$_{50}$ = 0.034 ± 0.008, Figure 3a) nor DPCPX (EC$_{50}$ = 0.048 ± 0.006, Figure 3b) seemed to influence the inotropic effect of **5b**.

3D QSAR Study Using GRIND Descriptors. Molecular modeling techniques were applied to gain further insight into the structure−activity relationships of the acetals described above. CEBs presented in refs 3 and 11 were additionally included in the dataset to enlarge its chemical diversity. For all compounds with a basic center the pK_a was evaluated by means of the CXCALC calculator plug in of the program JCHEM.[29] Compounds **8c**, **11d**, and **24b** from the training set as well as compounds **10d**, **11g**, **13**, and **24a** from the test set revealed calculated pK_a values greater than that of diltiazem, the experimental value of which is 7.7.[30] Hence, they were modeled in their nitrogen-protonated cationic form. Details are reported in the Supporting

Table 4. Molecules Selected for the 3D QSAR Study (training set)

Scaffold 1[a]   **Scaffold 2**[a]   **Scaffold 3**[a]

	scaffold	R1	R2	R	R	R	pEC$_{50}$[b]
4B[c]	1	Cl	H	H	H	H	−0.610
4C[c]	1	Cl	H	H	CH$_3$	CH$_3$	−0.152
4I[c]	1	C$_6$H$_5$	H	H	H	CH$_3$	−0.423
4L[c]	1	NO$_2$	H	H	H	CH$_3$	−0.217
4N[c]	1	H	CH$_3$	H	H	CH$_3$	0.143
4P[c]	1	H	NO$_2$	H	H	CH$_3$	−0.246
4Q[c]	1	H	CF$_3$	H	H	CH$_3$	−0.336
6[c]	1	H	H	H	H	CH$_3$	−0.818
1a[c]	1	Cl	H	H	H	CH$_3$	0.097
1b[c]	1	Br	H	H	H	CH$_3$	0.495
5a	1	Cl	H	CH$_2$CH$_3$	H	CH$_3$	0.569
5b	1	Br	H	CH$_2$CH$_3$	H	CH$_3$	1.398
10b	1	Br	H	(CH$_2$)$_8$CH$_3$	H	CH$_3$	0.456
11b	1	Br	H	(CH$_2$)$_{11}$CH$_3$	H	CH$_3$	0.886
12b	1	Br	H	(CH$_2$)$_{14}$CH$_3$	H	CH$_3$	0.377
13b	1	Br	H	(CH$_2$)$_{17}$CH$_3$	H	CH$_3$	0.013
14a	1	Cl	H	CH(CH$_3$)$_2$	H	CH$_3$	0.658
18a	1	Cl	H	(CH$_2$)$_8$CH=CH(CH$_2$)$_7$CH$_3$ (Z-isomer)	H	CH$_3$	0.060
18b	1	Br	H	(CH$_2$)$_8$CH=CH(CH$_2$)$_7$CH$_3$ (Z-isomer)	H	CH$_3$	−0.100
20a	1	Cl	H	CH$_2$-cyclohexyl	H	CH$_3$	0.620
20b	1	Br	H	CH$_2$-cyclohexyl	H	CH$_3$	0.721
8c[d]	2	H	H	CH$_2$N(CH$_3$)$_2$			−0.176
11d[d]	2	OCH$_3$	H	3,4-(OCH$_3$)$_2$C$_6$H$_3$CH$_2$CH$_2$NHCH$_2$			0.347
22a[d]	2	H	OCOCH$_3$	H			0.420
24b[d]	2	OCH$_3$	4OCH$_3$C$_6$H$_4$	CH$_2$N(CH$_3$)$_2$			0.137
28b[d]	3						−0.079

[a] *S*-Enantiomers were used for modeling dataset compounds with the exception of compound **28b**, which was used as the *S,S*-isomer even if its potency is referred to the racemic form;[11] further details are given in the Supporting Information. [b] Negative inotropic potency pEC$_{50}$ calculated as −log EC$_{50}$, where EC$_{50}$ (μM) values of inotropic negative activity were computed from log concentration−response curves (Probit analysis according to Litchfield and Wilcoxon[22] with $n = 6-8$) as reported in Table 1 and ref 3; for data taken from ref 11 $n = 5-7$. [c] Molecule and data taken from ref 3. [d] Molecule and data taken from ref 11.

Information. Dataset compounds were minimized in vacuo with the program SYBYL[31] by using the procedure CONCORD.[32] Whereas synthesis and pharmacological measurements apply to the racemic compounds, a homologuous set of *S*-enantiomers was used for modeling. In fact, the molecular descriptors summarized below are independent of the molecular alignment and from the *R/S* character when almost all the molecular structures present a single stereogenic center. Detailed proof is supplied as Supporting Information.

The 3D QSAR study was performed by means of molecular descriptors derived from molecular interaction fields (MIF) which were computed on the basis of the GRID force field.[19,20] GRID MIF are suitable to address cases of unknown receptor binding sites. For this purpose, a novel method has been recently developed to encode MIF into molecular descriptors, independent from the superimposition of the set of compounds. This novel procedure, called GRIND, is commonly used in the absence of binding site knowledge; therefore, it was applied to the set of compounds presented above.

The BTZ binding site was mimed by using the GRID probes DRY, O::, and N1, which simulate the presence of lipophilic regions (DRY) and hydrogen bonding (HB) acceptors (O::) and donors (N1) around the molecule. A

Table 5. Values of r^2 and q^2 with Two Validation Schemes, Leave One Out and Leave 20% Out, and Sdep for the External Test Set for the First Three Latent Variables (LV) of the PLS Model

		q^2		
LV	r^2	loo[a]	l20%o[b]	sdep
1	0.67	0.42	0.37	0.21
2	0.82	0.66	0.63	0.18
3	0.84	0.66	0.65	0.21

[a] Cross−validation parameters: max dimensionality = 5; with recalculated weights; validation mode by leave-one-out. [b] Cross−validation parameters: max dimensionality = 5; with recalculated weights; validation mode by random groups; number of groups = 5; number of sdep = 20.

supplementary probe, called TIP, describing the molecular shape in terms of bulk and elongation,[33] was added to the analysis. The MIF obtained were encoded into the mentioned GRIND descriptors by means of the program ALMOND:[34] the entire set of molecules was described by 870 descriptors, which composed the X-data matrix used for statistical analysis. More details on the GRIND descriptors are available in the Experimental Section.

A principal component analysis (PCA) was carried out to classify the dataset compounds according to their 3D structures into clusters. To span the largest range of
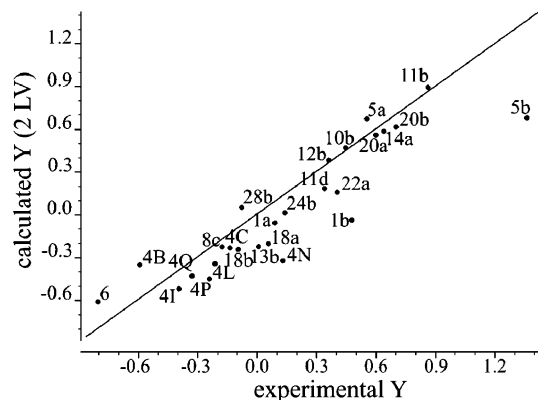
Figure 4. Calculated (2 LV) versus experimental values of inotropic activity, expressed as pEC$_{50}$.
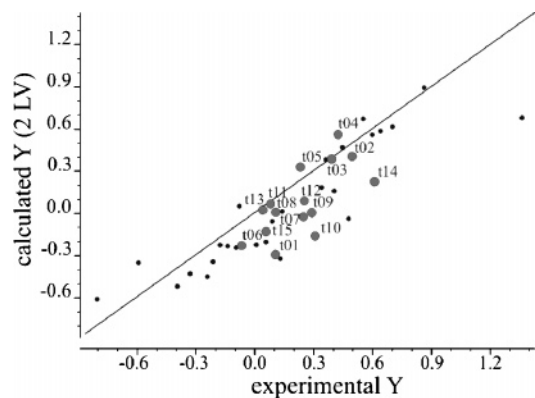

Figure 5. Calculated (2 LV) versus experimental values of inotropic activity, expressed as pEC$_{50}$. The training set is reported as black points, whereas the test set is marked as gray labeled points.
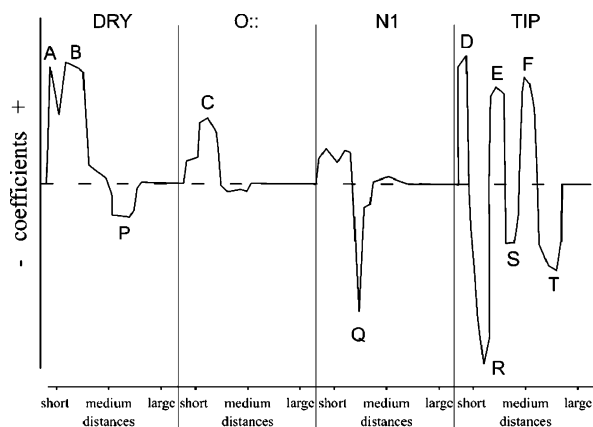

Figure 6. Profile of PLS coefficients for the 3D QSAR model. For the four blocks of descriptors the correlation with the inotropic activity is shown. Positive or negative coefficient values indicate, respectively, direct or inverse correlation with the activity. Furthermore, large values mean strong impact, while slight values mean marginal impact. Groups of contiguous variables with a strong positive (A, B, C, D, E and F) or inverse (P, Q, R, S, and T) correlation with the activity are marked with capital letters.
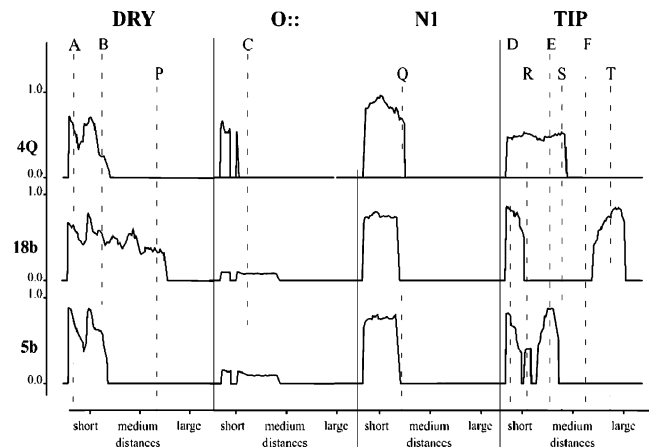
Figure 7. Profile of the most important variables (blocks DRY, O::, N1, and TIP) for the compounds **4Q**, **18b**, and **5b**, which present low, medium, and high potency, respectively. Peaks A and B belong to the probe DRY and correspond to the presence/absence of a generic alkyl group on the chain at C-8: a small chain (**5b**) favorably affects the activity, whereas the long lipophilic chain of **18b** negatively correlates with the activity (negative peak P). Probe O:: mimes the interaction with a hydrogen-bond acceptor like negatively charged carboxylic oxygen of Asp or Glu. Compounds **5b** and **18b** do not contain donor groups and their description resembles a plateau, whereas compound **4Q** presents a donor hydroxyl group. However, its peak was left-shifted with respect to the peak C, which was related to basic nitrogens. The negative peak Q from probe N1 involves MIF produced by the oxygen at position 8. The hydroxyl oxygen of the less active compound **4Q** has stronger acceptor character despite ether oxygens of **5b** and **18b**; thereby, it causes the most attractive MIF and its interactions are the highest in correspondence of the negative peak Q. The TIP probe extracts molecular shape information. The peak marked as D refers specifically to a methyl group bound to the skeleton or at the end of the acetal chain at C-8. The peak R, inversely related to the activity, mainly involves groups such as NO$_2$ and CF$_3$ meta-substituted on the phenyl ring at position 8. The peak E corresponds to the *p*-Cl/*p*-Br at the phenyl ring and to the small or moderately branched alkyl groups at the acetal chain, namely ethyl or isopropyl. Peaks S, F, and T correspond to the presence of *p*-halo-substituted phenyl edge and the end of the long chains at position 8: peak F exactly fits the correlogram of **11b**, which was the most active compound within the long-chain series. On the contrary, longer (**12b**, **13b**, **18a**, **18b**) lipophilic chains fit the peak T.

inotropic potencies, expressed as pEC$_{50}$, are given in Table 4 as compared to diltiazem (**2**).

Molecular descriptors were related to the inotropic potency by means of partial least squares (PLS) analysis. Fractional factorial design (FFD)[35] was used to select the variables for the X-space, which finally amounted to 460 GRIND descriptors. The optimum number of PLS components was chosen by monitoring the changes in the predictivity index (q^2) of the model, obtained by cross-validation procedures (leave one out and leave 20% out). The PLS model using two latent variables was optimal, as evinced by the r^2 and q^2 values for both cross-validation procedures (see Table 5).

Details of the model are reported in Figure 4, where the calculated negative inotropic potencies are plotted versus the experimental ones. To validate the model, a miscellaneous set of homologous compounds was extracted from the extended dataset already described. Biological data and 2D structures are available as

negative inotropic potency, representative molecules were selected from each cluster, taking into account the population of clusters as well as the pharmacological profile of compounds. The balanced training set was composed of 26 compounds; their 2D structures are available as Supporting Information. The negative
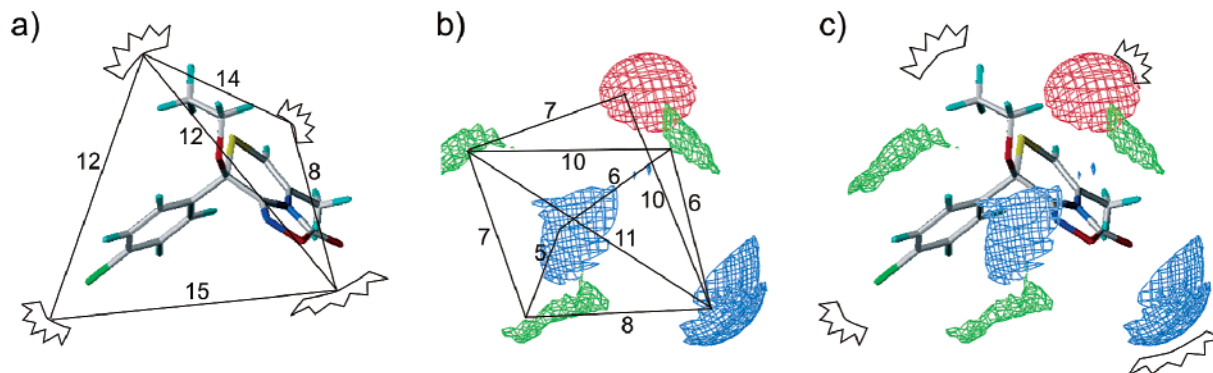
Figure 8. The virtual receptor scheme obtained from statistical analysis of GRIND descriptors presented with the most potent compound **5b**. Distances are expressed in Å. (a) Molecular edges, extracted from the probe TIP, are reported as crown-type symbols. (b) Hydrophobic regions (from the probe DRY) are green; hydrogen-bond-donor regions (from the probe N1) are blue; negatively charged and/or hydrogen-bond-acceptor regions (from the probe O::) are red. (c) Miscellaneous representation of pharmacologically important regions and molecular tips extracted from the model, presented with the compound **5b**.

Supporting Information. The prediction of the validation set is graphically represented in Figure 5: all the compounds were satisfactorily predicted.

To gain a deeper insight into the model, we inspected in more detail those variables with high positive or negative impact on inotropic potency. In the PLS coefficient profile reported in Figure 6 groups of variables are referred to as peaks labeled with capital letters.

For a better understanding, it is worth mentioning that GRIND variables refer to inter-MIF distances, while each MIF represents a point around the molecule with a specific value of attractive interaction between the entire molecule and the probe. Therefore, a variable that is referred to as DRY−DRY represents a pair of MIF, both obtained with the probe DRY and exhibiting a specific mutual distance.

Thus, peak A represents two DRY MIF 3 Å apart, whereas peak B represents two DRY MIF 9 Å apart. These distances and the following ones show positive correlation with inotropic potency: 9 Å between two O:: MIF and 3, 13, and 20 Å between pairs of TIP points. Conversely, peak P represents two DRY MIF 23 Å apart; this peak and peaks Q (N1−N1, 12 Å), R, S, and T (TIP−TIP, 7, 17, 28 Å) exhibit a strong inverse correlation to the inotropic potency. The high values of some distances are due to the large size of some acetal chains. All of these peaks are discussed in Figure 7 to highlight the differences between the weakly potent compound **4Q**, the intermediate **18b**, and the highly potent **5b**.

The final step of this analysis was the construction of a virtual receptor site (VRS), obtained by combining the most relevant GRIND variables with positive impact. These were back-encoded into the relevant MIF around the molecules, which can be viewed as pharmacophoric regions of a virtual receptor. The latter is completed by a set of distances between the mentioned pharmacophoric regions, as presented in Figure 8. The virtual receptor scheme extracted in this way comprises three hydrophobic regions, two HB donor regions, and one HB acceptor/negatively charged region. Encoding this scheme into molecules, a good negative inotropic profile was likely to arise from three lipophilic groups, two HB acceptor groups, and one basic center. Peaks involving the TIP probe were used to assign edges to

the 3D scheme and to confirm location of the aforementioned regions. MIF regions, molecular edges, and distances between them are presented together in Figure 8 for compound **5b**.

Taken together, the combined 3D QSAR/VRS approach allowed us to define six crucial pharmacophoric features that favorably affect the negative inotropic potency:

(i) a small alkyl chain, such as ethyl or *i*-propyl, bound to the ether oxygen at position 8;

(ii) a methyl at position 5;

(iii) a weak hydrogen-bond acceptor at position 8, likewise the ether oxygen;

(iv) *para*-substituents on the phenyl ring at position 8;

(v) a large hydrophilic region with hydrogen-bond-accepting character in correspondence to the oxygen from the oxadiazolone moiety; and

(vi) a basic center, such as nitrogen, which is modeled in its protonated form.

These positive requirements are in agreement with the proposals of other groups.[13−15]

In addition, from the QSAR model we could define three features that unfavorably affect the negative inotropic potency:

(i) OH instead of ether oxygen at position 8,

(ii) *meta*-substituents on the phenyl ring at position 8, and

(iii) lipophilic chains bound to the ether oxygen at position 8 longer than 12 carbon atoms.

The developed quantitative model can be used to forecast the negative inotropic potency of further analogues of hypothetical BTZ-type calcium antagonists, whereas the 3D pharmacophore scheme could be used for fast recognition of potential CEB structurally similar to the series presented.

Conclusions

The cardiovascular characterization of a series of new synthesized compounds is reported in this paper. They show a negative inotropic effect on isolated tissues without affecting chronotropy or vasorelaxant activity. **5b** elicited a potent negative inotropic activity about 20-fold more potent than diltiazem, which shows poor selectivity between inotropy, chronotropy, and vasculature. The specific and selective cardiac effects of **5b**

were also confirmed by experiments performed on the left papillary muscle and on the isolated perfused heart according to Langendorff.

Moreover, selective functional assays excluded other receptor implications (M_2- and A_1-agonism) and suggested these compounds as specific ligands for cardiac L-type calcium channels. The cardiac selectivity could be explained by the different mechanisms that elicited contraction in the atria and ventricular muscle or by taking into account the attractive hypothesis of the existence of different L-type calcium channels expressed in these tissues.

Recently, a large-scale expression profile of ionic channels in different regions of the heart including the sinoatrial node, the atrial–ventricular node, the atrium, and the ventricle was described.[8,36] Clearly further studies are required to demonstrate whether the compounds studied in this paper interact with the multiple subtypes of calcium channels expressed in the heart.

A 3D QSAR study over a balanced dataset allowed a predictive PLS model to be developed. It was validated using homologous literature data and it would act as a guideline to prioritizing further derivatives before their synthesis and biological testing. In addition, a virtual receptor scheme derived by the 3D QSAR study demonstrated that a good negative inotropic profile was likely to arise from the presence of one basic center, three lipophilic groups, and two HB acceptor groups within the molecules. This 3D pharmacophoric model could be used as an "in silico" filter, to prioritize new synthetic work and contribute to guiding the development of new potent and selective compounds.

Experimental Section

Chemistry. ^{1}H and ^{13}C NMR spectra were recorded on a Varian Gemini 300 Instrument in the Fourier transform mode at 21 ± 0.5 °C in DMSO-d_6. Chemical shifts (δ) are in parts per million (ppm) from tetramethylsilane and coupling constants are in hertz. EI mass spectra of several compounds were recorded on a VG70 70E apparatus. ESI mass spectra were obtained on a micromass ZMD Waters instrument (30 V, 3.2 kV, isotope observed ^{35}Cl and ^{79}Br). Melting points were determined on a Kofler apparatus and are uncorrected. Solvents were removed under reduced pressure. Silica gel plates (Merck F_{254}) and silica gel 60 (Merck 230–400 mesh) were used for analytical TLC and for column chromatography, respectively. Compounds **1a**,[1] **1b**,[1] **3a**,[3] and **4a**[3] were obtained as previously reported. Melting points, yields, reaction times, and purification methods of all compounds are reported in Table 6. In every case an analytical sample of crystalline compounds (colorless crystals) was obtained by crystallization from EtOH/H_2O. All new compounds gave satisfactory microanalyses (C, H, N).

8-(4-Bromophenyl)-8-methoxy-5-methyl-8H-[1,4]thiazino[3,4-*c*][1,2,4]oxadiazol-3-one (3b). Trimethylorthoformate (0.4 mL, 3.2 mM) and *p*-toluenesulfonic acid (100 mg) were added to a solution of **1b** (273 mg, 0.8 mM) in MeOH (5 mL) and anhydrous toluene (5 mL). The solution was refluxed for 24 h, cooled to room temperature, and then poured into a saturated solution of NaHCO$_3$ (50 mL). The organic layer was separated and the water was extracted with CH$_2$Cl$_2$ (3 × 10 mL). The extracts were dried over Na$_2$SO$_4$, and the solvent was removed. ^{1}H NMR: δ 2.40 (3H, d, J = 1.3 Hz, 5-CH$_3$), 3.25 (3H, s, OCH$_3$), 6.21 (1H, q, J = 1.3 Hz, H-6), 7.52 (2H, part AA′ of the AA′XX′ system, H–Ar), 7.72 (2H, part XX′ of the AA′XX′ system, H–Ar). ^{13}C NMR: δ 16.3 (q, 5-CH$_3$), 52.0 (q, OCH$_3$), 82.6 (s, C-8), 102.8 (d, C-6), 123.2 (s, C-4′), 129.5 (d, C-2′, C-6′), 129.6 (s, C-5), 131.6 (d, C-3′, C-5′), 132.1 (s, C-1′), 154.0 (s, C-8a), 154.4 (s, C-3). EI: *m/z* (%) 356–354 (M$^+$, 66),

Table 6. Physical Data of Compounds 3a,b−20a,b

compd	reaction time (h)	yield (%)[a]	purificn method[b]	mp (°C)	HRMS calc/found
3a[c]	24	80	A	131−132	310.0179/310.0184[d]
3b	24	69	B	149−151	353.9674/353.9675[e]
4a[c]	3	72	A	122−123	352.0648/352.0654[d]
4b	4.8	50	A	133−134	396.0143/396.0146[e]
5a	2.5	59	A	86−87	324.0335/324.0334[d]
5b	3.3	70	A	120−121	367.9830/367.9835[e]
6a	4	59	B	89−90	338.0487/338.0489[d]
6b	4	56	B	116−117	381.9987/381.9984[e]
7a	3	54	B	55−56	352.0648/352.0644[d]
7b	5	43	A	89−90	396.0143/396.0142[e]
8a	3.5	77	B	107−108	366.0805/366.0807[d]
8b	3.5	78	B	114−115	410.0300/410.0305[e]
9a	5	66	B	66−67	380.0961/380.0958[d]
9b	6.5	59	B	71−72	424.0456/424.0453[e]
10a	2.5	77	B	90−91	422.1431/422.1433[d]
10b	5.3	69	B	81−82	466.0926/66.0929[e]
11a	3.2	50	A	59−60	464.1900/464.1902[d]
11b	3.5	70	A	48−49	508.1395/508.1393[e]
12a	3.2	85	A	62−63	506.2370/506.2374[d]
12b	3.2	86	A	55−56	550.1865/550.1863[e]
13a	3	78	A	67−68	548.2839/548.2834[d]
13b	3	69	A	64−65	592.2334/592.2337[e]
14a	8.5[f]	56	A	89−91	338.0492/338.0494[d]
14b	8.5[f]	57	A	104−105	381.9987/381.9990[e]
15a	2.5	68	B	108−109	336.0335/336.0332[d]
15b	4	66	B	120−121	379.9830/379.9827[e]
16a	6	59	A	76−77	364.0648/364.0646[d]
16b	7.5	70	A	82−83	408.0143/408.0148[e]
17a	5	71	A	65−67	364.0648/364.0645[d]
17b	6	71	A	76−78	408.0143/408.0147[e]
18a	4	96	A	yellow oil	546.2683/546.2685[d]
18b	4	81	A	yellow oil	590.2178/590.2174[e]
19a	3	78	A	141−142	386.0492/386.0495[d]
19b	4	69	A	131−132	429.9987/429.9984[e]
20a	3.5	93	A	93−94	392.0691/392.0696[d]
20b	3.5	81	A	103−104	436.0456/436.0458[e]

[a] Yields referred to isolated and purified material. *[b]* A, column flash chromatography (ethyl acetate:petroleum ether = 1:5 v/v as eluant) on SiO$_2$; B, crystallization from EtOH/H$_2$O. *[c]* Reference 3. *[d]* ^{35}Cl isotope. *[e]* ^{79}Br isotope. *[f]* The reaction was carried on at 90 °C.

325−323 (51), 297−295 (12), 281−279 (33), 224 (15), 200 (23), 185−183 (100), 157−155 (90), 104 (11), 99 (16), 91 (18), 76 (67), 75 (54), 72 (37), 71 (51), 67 (16), 50 (37), 45 (53). ESI: *m/z* 377.2 (M + Na$^+$).

General Procedure for the Synthesis of 5a–13a, 4b–13b, 15a–20a, 15b–20b. The appropriate primary alcohol (8 mM) and *p*-toluenesulfonic acid (20 mg) were added to a suspension of **1a** or **1b** (0.8 mmol) in anhydrous toluene (25 mL). The solution was refluxed until disappearance of **1**, cooled to room temperature, and then poured into a saturated solution of NaHCO$_3$ (50 mL). The organic layer was separated and the water was extracted with toluene (3 × 20 mL). The extracts were dried over Na$_2$SO$_4$, and the solvent was removed.

General Procedure for the Synthesis of 14a and 14b. 2-Propanol (15 mM) and *p*-toluenesulfonic acid (20 mg) were added to a suspension of **1a** or **1b** (0.8 mM) in anhydrous toluene (25 mL). The solution was kept at 90 °C until disappearance of **1**, cooled to room temperature, and then poured into a saturated solution of NaHCO$_3$ (50 mL). The organic layer was separated and the water was extracted with toluene (3 × 20 mL). The extracts were dried over Na$_2$SO$_4$, and the solvent was removed.

^{1}H NMR, ^{13}C NMR, ESI-MS, and EI-MS data for compounds **5a–20a** and **3b–20b** are available as Supporting Information in Table S8.

Pharmacology. 1. Guinea Pig Atrial Preparations. Female guinea pigs (300–400 g) were sacrificed by cervical dislocation. After thoracotomy the heart was immediately removed and washed by perfusion through the aorta with oxygenated Tyrode solution of the following composition

(mM): 136.9 NaCl, 5.4 KCl, 2.5 CaCl$_2$, 1.0 MgCl$_2$, 0.4 NaH$_2$PO$_4$·H$_2$O, 11.9 NaHCO$_3$, and 5.5 glucose. The physiological salt solution (PSS) was buffered at pH 7.4 by saturation with 95% O$_2$−5% CO$_2$ gas, and the temperature was maintained at 35 °C. Isolated guinea pig heart preparations were used: spontaneously beating right atria and left atria driven at 1 Hz. For each preparation, the entire left and right atria were dissected from the ventricles, cleaned of excess tissue, and hung vertically in a 15 mL organ bath containing the PSS continuously bubbled with 95% O$_2$−5% CO$_2$ gas at 35 °C, pH 7.4. The contractile activity was recorded isometrically by means of a force transducer (FT 0.3, Grass Instruments Corp., Quincy, MA) using Power Lab software (AD-Instruments Pty Ltd, Castle Hill, Australia). The left atria were stimulated by rectangular pulses of 0.6−0.8 ms duration and about 50% threshold voltage through two platinum contact electrodes in the lower holding clamp (Grass S88 Stimulator). The right atrium was in spontaneous activity. After the tissue was beating for several minutes, a length−tension curve was determined, and the muscle length was maintained to elicit 90% of maximum contractile force observed at the optimal length. A stabilization period of 45−60 min was allowed before the atria were used to test compounds. During the equilibration period, the bathing solution was changed every 15 min and the threshold voltage was ascertained for the left atria. Atrial muscle preparations were used to examine the inotropic and chronotropic activity of the compounds (0.01, 0.05, 0.1, 0.5, 1, 5, 10, 50, and 100 μM), first dissolved in DMSO and then diluted with PSS. According to this procedure, the concentration of DMSO in the bath solution never exceeded 0.3%, a concentration that did not produce appreciable inotropic and chronotropic effects. During the construction of cumulative dose−response curves, the next higher concentration of the compounds was added only after the preparation reached a steady state.

The selective functional assays were carried out on the left atria. These tissues were set up rapidly under a suitable tension in 15 mL organ baths containing PSS kept at the appropriate temperature (see above). Tissues were equilibrated for 60 min, and a cumulative-response curve to **5b** was constructed after incubation for 60 min with the antagonist atropine (1 μM) or DPCPX (1 μM).

2. Guinea Pig Left Papillary Muscle. The left ventricular papillary muscles were rapidly isolated from the heart and suspended in a organ bath (15 mL) containing modified Ringer solution of the following composition (mM): 135 NaCl, 5 KCl, 2 CaCl$_2$, 1 MgCl$_2$, 15 NaHCO$_3$, and 5.5 glucose, equilibrated with 95% O$_2$−5% CO$_2$ gas at pH 7.4 and maintained at 35 °C. The papillary muscles were driven through a pair of platinum electrodes (field stimulation) by square pulses (1 Hz, 5−7 ms, 50% threshold voltage). The developed tension was recorded isometrically. The preparation was equilibrated for at least 60 min before the start of the experiment.

3. Guinea Pig Aortic Strips. The thoracic aorta was removed and placed in Tyrode solution of the following composition (mM): 118 NaCl, 4.75 KCl, 2.54 CaCl$_2$, 1.20 MgSO$_4$, 1.19 KH$_2$PO$_4$, 25 NaHCO$_3$, and 11 glucose equilibrated with 95% O$_2$−5% CO$_2$ gas at pH 7.4. The vessel was cleaned of extraneous connective tissue. Two helicoidal strips (10 mm × 1 mm) were cut from each aorta beginning from the end most proximal to the heart. Vascular strips were then tied with surgical thread (6−0) and suspended in a jacketed tissue bath (15 mL) containing aerated pharmacological salt solution (PSS) at 35 °C. Strips were secured at one end to a force displacement transducer (FT 0.3, Grass Instruments Corp.) for monitoring changes in isometric contraction. Aortic strips were subjected to a resting force of 1 g and washed every 20 min with fresh PSS for 1 h after the equilibration period; guinea pig aortic strips were contracted by washing in PSS containing 80 mM KCl (equimolar substitution of K$^+$ for Na$^+$). After the contraction reached a plateau (about 45 min) the compounds (0.1, 0.5, 1, 5, 10, 50, and 100 μM) were added cumulatively to the bath allowing for any relaxation to obtain an equilibrated level of

force. Addition of the drug vehicle had no appreciable effect on K$^+$-induced contraction (DMSO for all compounds).

4. Guinea Pig Isolated Perfused Heart According to Langendorff. Female guinea pigs (300−400 g) were killed by cervical dislocation. The heart were quickly removed and rapidly perfused through the aorta at constant flow (11−12 mL min^{-1} g^{-1}) with a modified Krebs−Henselait solution with the following composition (mM): 128 NaCl, 4.7 KCl, 2.5 CaCl$_2$, 1.2 MgSO$_4$, 15 NaHCO$_3$, 1.2 KH$_2$PO$_4$, 11.1 glucose, and 2 Na pyruvate, bubbled with a gas mixture (95% O$_2$−5% CO$_2$) (pH = 7.4−7.5) and maintained at 37 °C. A perfusion pressure of 50−60 mmHg was obtained at this flow rate. The addition of pyruvate to the medium has been shown to confer to the isolated heart the same metabolic and functional features of the heart in situ.[37] A stabilization period of 30 min was given to the heart, under normal electrocardiogram (ECG) conditions, to keep the frequency of spontaneous beating hearts constant at 210 ± 3 beats min^{-1}. Surface ECG was recorded by means of two electrodes, placed one near the initial portion of the anterior intraventricular artery and the other on the left ventricular free wall. The main ECG intervals (PR = atrioventricular conduction time; QRS = intraventricular conduction time; JT = duration of ventricular depolarization) were measured. The drug-induced changes in conduction velocity of AV node and ventricular myocardium were calculated as changes in the reciprocal of the PR interval and QRS interval, respectively.[38] Heart contractility was measured, by means of intraventricular latex balloon, as the positive peak of the first derivative of the left ventricular pressure as a function time [+(dP/dt)$_{max}$]. Coronaric perfusion pressure (CPP) (mmHg) was measured to assess the change in coronary vessel resistance. The compounds were added with increasing concentrations (0.001, 0.01, 0.1, 1 μM). During the building of concentration−response curves, the next higher concentration of the compounds was added only after the preparation reached a steady state (about 30 min). The potency of drugs, defined as pEC$_{50}$ value, was evaluated from log concentration−response curves (n = 6−8),[23,24] in the appropriate pharmacological preparations. All data are presented as mean ± SEM.[24]

Molecular Modeling. GRIND descriptors. GRIND[21] were generated, analyzed, and interpreted using the software ALMOND, version 3.2.[34] GRIND have been designed mainly to represent pharmacodynamic properties; they start from molecular interaction fields (MIF) computed on the basis of the GRID force field.[19,20] When MIF are computed for the database molecules, the regions showing favorable energies of interaction represent positions where groups of a hypothetical receptor would interact favorably with a dataset molecule. Using different probes, a set of such positions would define a virtual receptor site (VRS). Basically, GRIND are a small set of variables representing the geometrical relationships between relevant regions of the VRS. The procedure for obtaining GRIND involves three steps: (a) computing a set of MIF, (b) filtering the MIF to extract the most relevant regions, and (c) encoding the filtered MIF into the GRIND variables. These variables represent the product of the field energy of node-pairs that are separated by certain distances in the 3D space of each compound. GRIND variables are organized in correlograms either representing node-pairs of the same field (autocorrelograms, presented in Figure 6) or node-pairs of different fields (cross-correlograms). The alignment-independent GRIND, obtained in this way, were used directly for the chemometric analysis and were interpreted with the software ALMOND in interactive 3D plots together with the molecular structures.

Statistical Analysis. Principal component analysis (PCA) and partial least squares (PLS) analysis were performed within the software ALMOND[34] on the unscaled data matrix. PCA was used to cluster the compounds, with the aim of extracting a balanced set of molecules with the largest amount of information. The selected compounds are listed in Table 4. PLS was used in order to maximize the relationship between the GRIND descriptors and the inotropic potency expressed as −log EC$_{50}$ (pEC$_{50}$). The optimal dimensionality of the PLS

model was chosen according to cross-validation analysis, using the leave one out (LOO) and five random groups out (leave 20% out) procedures. The following setting was used for the variable selection via fractional factorial design (FFD):[27] max dimensionality = 2; with recalculated weights; validation mode by random groups; number of groups = 5; number of SDEP = 20; retain uncertain variables; percentage of dummies = 20%; combinations/variables ratio = 2. Two runs were executed. The number of descriptors was reduced to 460 by zeroing all the variables with negative impact on the model predictivity. All computations were run on Silicon Graphics SGI O2 R10000 and R12000 workstations.

Supporting Information Available: Calculated pK_a values; description of the two enantiomers (*R* and *S*) for compound **20b**; 2D-structures and data for compounds of both training set and test set; the ^{1}H, ^{13}C NMR, ESI-MS, and EI-MS data. This material is available free of charge via the Internet at http://pubs.acs.org.

References

(1) Billi, R.; Cosimelli, B.; Spinelli, D.; Rambaldi, M. Ring−ring Interconversion. Part 2. Effect of the Substituents on the Rearrangement of 6-Aryl-3-methyl-5-nitrosoimidaz[2,1-*b*][1,3]-thiazoles into 8-Aryl-8-hydroxy-5-methyl-8*H*-[1,4][3,4-*c*][1,2,4]-oxadiazol-3-ones. A Novel Class of Potential Antitumor Agents. *Tetrahedron* **1999**, *55*, 5433−5440.

(2) Billi, R.; Cosimelli, B.; Leoni, A.; Spinelli, D. Ring−ring Interconversion. Part 3. On the Effect of the Substituents on the Thiazole Moiety in the Ring-Opening/Ring-Closing Reactions of Nitrosoimidazo[2,1-*b*][1,3]thiazoles with Hydrochloric Acid. *J. Heterocycl. Chem.* **2000**, *37*, 875−878.

(3) Budriesi, R.; Cosimelli, B.; Ioan, P.; Lanza, C. Z.; Spinelli, D.; Chiarini, A. Cardiovascular Characterization of [1,4]Thiazino-[3,4-*c*][1,2,4]oxadiazol-1-one derivatives: Selective Myocardial Calcium Channel Modulators. *J. Med. Chem.* **2002**, *45*, 3475−3481.

(4) Schleifer, K.-J. Selective Characterization of 1,4-Dihydropyridine Binding Site at L-type Calcium Channels in the Resting State and the Opened/Inactivated State. *J. Med. Chem.* **1999**, *42*, 2204−2211.

(5) Jones, S. W. Overview of Voltage-Dependent Calcium Channels. *J. Bioenerg. Biomembr.* **1998**, *30*, 299−312.

(6) Striessnig, J.; Grabner, M.; Mitterdorfer, J.; Hering, S.; Sinnegger, M. J.; Glossmann, H. Structural Bases of Drug Binding to L-Ca^{2+} Channels. *TiPS* **1998**, *19*, 108−115.

(7) Catterall, W. A. Structure and Regulation of Voltage-Gated Ca^{2+} Channels. *Annu. Rev. Cell. Dev. Biol.* **2000**, *16*, 521−555.

(8) Hu, H.; Marban, E. Isoform-Specific Inhibition of L-Type Calcium Channels by Dihydropyridines Is Independent of Isoform-Specific Gating Properties. *Mol. Pharmacol.* **1998**, *53*, 902−907.

(9) Ertel, E. A.; Campbell, K. P.; Harpold, M. M.; Hofmann, F.; Mori, Y.; Perez-Reyes, E.; Swartz, A.; Snutch, T. P.; Tanabe, T.; Birnauber, L.; Tsien, R. W.; Catterall, W. A. Nomenclature of Voltage-Gated Calcium Channels. *Neuron* **2000**, *25*, 533−535.

(10) Kimball, S. D.; Floyd, D. M.; Das, J.; Hunt, J. T.; Krapcho, J.; Rovnyak, G.; Duff, K. J.; Lee, V. G.; Moquin, R. V.; Turk, C. F.; Hedberg, S. A.; Moreland, S.; Brittain, R. J.; McMullen, D. M.; Normandin, D. E.; Cucinotta, G. G. Benzazepinone Calcium Channel Blockers. 4. Structure−Activity Overview and Intracellular Binding Site. *J. Med. Chem.* **1992**, *35*, 780−793.

(11) Campiani, G.; Garofalo, A.; Fiorini, I.; Botta, M.; Nacci, V.; Tafi, A.; Chiarini, A.; Budriesi, R.; Bruni, G.; Romeo, M. R. Pyrrolo-[2,1-*c*][1,4]benzothiazines: Synthesis, Structure−Activity Relationships, Molecular Modeling Studies and Cardiovascular Activity. *J. Med. Chem.* **1995**, *38*, 4393−4410.

(12) Campiani, G.; Nacci, V.; Fiorini, I.; De Filippis, M. P.; Garofalo, A.; Ciani, S. M.; Greco, G.; Novellino, E.; Williams, D. C.; Zisterer, D. M.; Woods, M. J.; Mihai, C.; Manzoni, C.; Mennini. T. Synthesis, Biological Activity, and SARs of Pyrrolobenzoxazepine Derivatives, a New Class of Specific "Pheripheral-Type" Benzodiazepine Receptor Ligands. *J. Med. Chem.* **1996**, *39*, 3435−3450.

(13) Corelli, F.; Manetti, F.; Tafi, A.; Campiani, G.; Nacci, V.; Botta, M. Diltiazem-like Calcium Entry Blockers: A Hypothesis of the Receptor-Binding Site Based on a Comparative Molecular Field Analysis Model. *J. Med. Chem.* **1997**, *40*, 125−131.

(14) Kettmann, V.; Höltje, H.-D. Mapping of the Benzothiazepine Binding Site on the Calcium Channel. *Quant. Struct.-Act. Relat.* **1998**, *17*, 91−101.

(15) Schleifer, K.-J.; Tot, E. Molecular Modeling Study of Diltiazem Mimics at L-Type Calcium Channels. *Pharmaceut. Res.* **1999**, *16*, 1506−1513.

(16) Coburn, R. A.; Wierzba, M.; Suto, M. J.; Solo, A. J.; Triggle, A. M.; Triggle, D. J. 1,4-Dihydropyridine Antagonist Activities at the Calcium Channel: A Quantitative Structure−Activity Relationship Approach. *J. Med. Chem.* **1988**, *31*, 2103-2107.

(17) Zamponi, G. W.; Stotz, S. C.; Staples, R. J.; Andro, T. M.; Nelson, J. K.; Hulubei, V.; Blumenfeld, A.; Natale, N. R. Unique Structure−Activity Relationship for 4-Isoxazolyl-1,4-dihydropyridines. *J. Med. Chem.* **2003**, *46*, 87−96.

(18) Hockerman, G. H.; Johnson, B. D.; Abbott, M. R.; Scheuer, T.; Catterall, W. A. Molecular Determinants of High Affinity Phenylalkylamine Block of L-type Calcium Channels in Transmembrane Segment IIIS6 and the Pore Region of the α$_1$ Subunit. *J. Biol. Chem.* **1997**, *272*, 18759−18765.

(19) (a) Goodford, P. J. A Computational Procedure for Determining Energetically Favorable Binding Sites on Biologically Important Macromolecules. *J. Med. Chem.* **1985**, *28*, 849−857. (b) Carosati, E.; Sciabola, S.; Cruciani, G. Hydrogen Bonding Interactions of Covalently Bonded Fluorine Atoms: From Crystallographic Data to a New Angular Function in the GRID Force Field. *J. Med. Chem.* **2004**, *47*, 5114−5125.

(20) Version 22 of the program GRID is available from Molecular Discovery Ltd., 215 Marsh Road, HA5 5NE, Pinner, Middlesex, UK, http://www.moldiscovery.com.

(21) Pastor, M.; Cruciani, G.; McLay, I.; Pickett, S.; Clementi S. GRid-INdependent descriptors (GRIND): A Novel Class of Alignment-Independent Three-Dimensional Molecular Descriptors. *J. Med. Chem.* **2000**, *43*, 3233−3243.

(22) Tallarida, R. J.; Murray, R. B. *Manual of Pharmacologic Calculations with Computer Programs*, 2nd ed.; Springer-Verlag: New York; 1987.

(23) Motulsky, H., Christopoulos, A. Fitting Models to Biological Data Using Linear and Non Linear Regression. www.GraphPad.com, 2003

(24) Motulsky H., Statistic Guide: Statistical Analysis for Laboratory and Clinical Research: A Pratical Guide to Curve Fitting. www.GraphPad.com, 2003

(25) Campiani, G.; Nacci, V.; Garofalo, A.; Botta, M.; Fiorini, I.; Tafi, A. Synthesis and Preliminary Biological Evaluation of 1-Aminomethyl-4-substituted-4*H*-pyrrolo[2,1-*c*][1,4]benzothiazines, A New Class of Calcium Antagonists. *Bioorg. Med. Chem. Lett.* **1992**, *2*, 1193−1198.

(26) Campiani, G.; Garofalo, A.; Fiorini, I.; Nacci, V.; Botta, M.; Tafi, A. Synthesis and "In Vitro" Cardiovascular Activity of 4-Aryl-2,3, 3a, 4-tetrahydro-1*H*-pyrrolo[2,1-*c*][1,4]benzothiazin-3-ones and 7-Acetoxy-6-phenyl-7a,8,9,10-tetrahydropyrrolo[2,1-*d*][1,5]-benzothiazepin-10-one. *Bioorg. Med. Chem. Lett.* **1994**, *4*, 1235−1240.

(27) Campiani, G.; Ramunno, A.; Fiorini, I.; Nacci, V.; Morelli, E.; Novellino, E.; Goegan, M.; Mennini, T.; Sullivan, S.; Zisterer, D. M.; Williams, C. D. Synthesis of New Molecular Probes for Investigation of Steroid Biosynthesis induced by Selective Interaction with Pheripheral Type Benzodiazepine Receptors (PBR). *J. Med. Chem.* **2002**, *45*, 4276−4281.

(28) Guernelli, S.; Laganà, M. F.; Mezzina, E.; Ferroni, F.; Siani, G.; Spinelli, D. Supramolecular Complex Formation: A Study of the Interactions between β-Cyclodextrin and Some Different Classes of Organic Compounds by ESI-MS, Surface Tension Measurements, and UV/Vis and ^{1}H NMR Spectroscopy. *Eur. J. Org. Chem.* **2003**, 4765−4776.

(29) JCHEM is available from ChemAxon Ltd., Máramaros köz 3/a Budapest, 1037 Hungary, http://www.chemaxon.com.

(30) Mazzo, D. J.; Obetz, C. L.; Shuster, J. Diltiazem Hydrochloride. *Anal. Profiles Drug Subst. Excipients* **1994**, *23*, 53−98.

(31) SYBYL 6.7, Tripos Inc., 1699 South Hanley Road, St. Louis, MO, 63144.

(32) CONCORD 4.0.7. Pearlman, R. S. CONCORD User's Manual; Distributed by Tripos, Inc., St. Louis, MO.

(33) Fontaine, F.; Pastor, M.; Sanz, F. Incorporating Molecular Shape into the Alignment-free GRid-INdependent descriptors (GRIND). *J. Med. Chem.* **2004**, *47*, 2805−2815.

(34) Version 3.2 of the Software ALMOND is available from Molecular Discovery Ltd., 215 Marsh Road, HA5 5NE, Pinner, Middlesex, UK, http://www.moldiscovery.com.

(35) Baroni, M.; Costantino, G.; Cruciani, G.; Riganelli, D.; Valigi, R.; Clementi, S. Generating Optimal Linear PLS Estimations (GOLPE): An Advanced Chemometric Tool for Handling 3D QSAR Problems. *Quant. Struct.-Act. Relat.* **1993**, *12*, 9−20.

(36) Marionneau, C.; Couette, B.; Liu, J.; Li, H.; Mangoni, M. E.; Nargeot, J.; Lei, M.; Escande, D.; Demolombe, S. Specific Pattern of Ionic Channel Gene Expression Associated with Pacemaker Activity in the Mouse Heart. *J. Physiol.* **2004**, DOI: 101113/jphysiol.2004.074047.

(37) Bunger, R. F. J.; Haddy, A.; Querengasser, E.; Gerlach, E. An Isolated Guinea-pig Heart Preparation with in vivo like Feature. *Pflügers. Arch.* **1975**, *353*, 317−326.

(38) Bova, S.; Cargnelli, G.; D'Amato, E.; Forti, S.; Yang, Q.; Trevisi, L.; Debetto, P.; Cima, L.; Luciani, S.; Padrini, R. Calcium-Antagonist Effects of Norbormide on Isolated Perfused Heart and Cardiac Myocytes of Guinea-pig: A Comparison with Verapamil. *Br. J. Pharmacol.* **1997**, *120*, 19−24.